Design and simulation of turbogenerators for series hybrid electric vehicles

Joseph Al Khoury, Wissam Bou-Nader

Energy Conversion and Management 236 (2021) 114078

Contents lists available at ScienceDirect

Energy Conversion and Management

journal homepage: www.elsevier.com/locate/enconman

Design and simulation of turbogenerators for series hybrid electric vehicles

Joseph Al Khoury *, Wissam Bou Nader

Groupe PSA, Centre Technique de Vélizy, Vélizy, France

ARTICLE INFO

Keywords:
Series hybrid electric vehicle
Turbogenerator
Thermodynamic
Turbomachine design
Recuperator
Dynamic modeling

ABSTRACT

To reduce emissions and fuel consumption in the automotive world, researchers are looking for alternative energy converters in the series hybrid electric vehicle and previous studies demonstrate that turbogenerator technologies are promising candidates. This study presents a methodology for the design, modelization, and dynamic simulation of different turbogenerator thermodynamic architectures to compare their performances, compute their efficiencies and select the best candidate to replace the internal combustion engine in the series hybrid electric vehicle taking into account the startup phase, where the inertia of the components affect the performance of the machine. Therefore, four types of turbogenerator configurations were thermodynamically investigated. Then an extensive work was conducted to design the turbomachines components with high efficiencies, followed by a design procedure of the recuperators. Dynamic models of the turbogenerators were developed and simulated with a constant power start-up strategy where the data of the designed components were integrated into the models. Results show that the turbogenerators that contain a recuperator have a startup phase characterized by high fuel consumption for 70 s mainly caused by the thermal inertia of the recuperator that causes a reduction in turbogenerators efficiencies by about 3%. Moreover, the intercooled regenerative reheated turbogenerator presented a better performance than the other turbogenerators with the highest rate of temperature increase at the inlet of the combustion chamber resulting in the lowest fuel consumption. Consequently, the intercooled regenerative reheated turbogenerator was selected as the best candidate as it had the best dynamic performance, the highest efficiency 37.9%, and net specific work 205 kJ/kg for a turbine inlet temperature of 950 °C. The developed methodology in this paper could be applied to reproduce new turbogenerator energy architectures, compare their performances, and select the best designs.

1. Introduction

Transport represents almost a quarter of Europe's greenhouse gas emissions and is the main cause of air pollution in cities [1]. With euro 6, regulations nowadays become more and more strict about emissions, by 2021 the average CO2 emissions in Europe should be below 95 g/km [2]. The electrification and hybridization of vehicles in the automotive industry is an efficient way to reduce the dependence of cars on oil. Since the fuel consumption of hybrid vehicles depends on the energy converter efficiency, much research invested in a new energy converter that has high efficiency and suitable for integration as an auxiliary power unit (APU) in the powertrains of hybrid vehicles [4,6,9].

Among energy converters, we enumerate the turbogenerator, the internal combustion engine (ICE), and polymer electrolyte membrane fuel cells (PEMFC). Turbogenerators operating in a series hybrid electric vehicle (SHEV) at a steady-state presents an optimum electric efficiency between 30.4% and 47% depending on the turbogenerator energy configuration meanwhile the maximum electric efficiency of a spark-ignition internal combustion engine (SI-ICE) APU is 36% [9]. On the other hand, the turbogenerator has several pluses over the ICE such as emission reduction, multi-fuel capability, fewer moving parts, less vibration, lower maintenance cost, high durability, and the absence of a cooling system [9,12]. PEMFC has also many advantages, like the highest efficiency (40–52%) among the APUs, zero tanks to wheel emission, and similar to the turbogenerator they have low noise and vibrations. Despite the many advantages of fuel cells, they are expensive due to too many reasons like, expensive Platine catalyst, expensive storage systems for hydrogen that must be safe and compact, fuel cell costs, and the cost of hydrogen refueling infrastructures.

The turbogenerator operating according to the gas turbine thermodynamic cycle or Brayton cycle has been largely investigated since the 1950s. Previous work in the turbogenerator hybrid vehicle area was theoretical, with one notable exception being the Volvo ECC which was shown in 1992 [5]. A study at the Chalmers University of Technology

* Groupe PSA, Technical Center of Vélizy, Vélizy, France.
E-mail addresses: joseph.al_khoury@mines-paristech.fr (J. Al Khoury), wissam.bounader@stellantis.com (W. Bou Nader).

https://doi.org/10.1016/j.enconman.2021.114078
Received 30 November 2020; Accepted 17 March 2021
Available online 5 April 2021

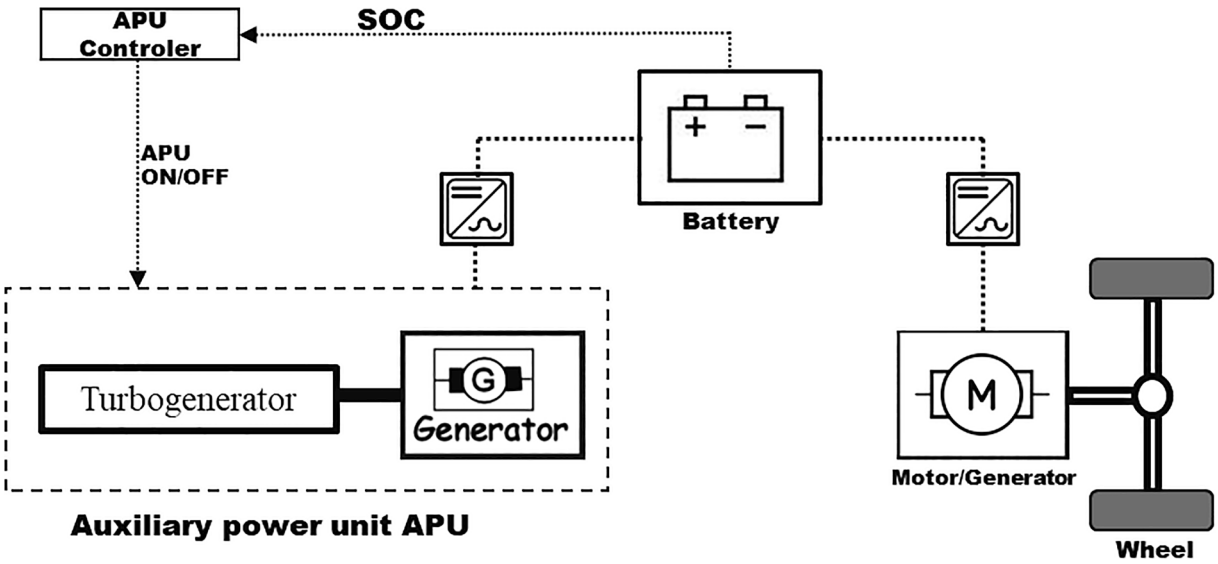

Fig. 1. Turbogenerator as an APU in the powertrain of SHEV.

showed the advantage of a turbogenerator operating at its optimal efficiency compared with the internal combustion engine in automotive applications [6]. Another one that was carried at the University of Rome proved that the turbogenerator, at its optimum efficiency, respects the Euro 6 emissions levels without the need for a pollution treatment system [7].

In conventional cars, the turbogenerator operating at partial loads suffering from low efficiency and inertia lag problems, gain interest again in the SHEV because the powertrains of these vehicles rely on an auxiliary power unit to charge the batteries that supply the electric motors to drives the vehicle (Fig. 1). The turbogenerator coupled to a generator constitutes the APU which is not mechanically connected to the driving wheels. This isolates the turbogenerator from demand, allowing it to consistently operate at its most efficient speed.

On the other side, many possible turbogenerator thermodynamics architectures can be integrated into the SHEV [9,10]. Some integrate a recuperator to increase the efficiency and benefits from the exhaust gas high temperature to preheat the combustion chamber inlet air [3]. Others integrate an intercooler between the compressor stages to decrease the power consumed by the compressor [11] and recently some works focused on the integration of a reheater or a post-combustion chamber between the turbine stages to increase the expansion power produced by the turbine [12].

Moreover, in the automotive world, cost, simplicity, and manufacturing complexity are important factors to consider besides the low emission and fuel economy. For this reason, the regenerative cycle got the highest interest and researches due to its good efficiency and its low complexity [4,8]. However, the regenerative cycle suffers from low net specific work leading to a high air mass flow rate [10] which consequently increases its size and weight. For this reason, recent studies show that the intercooled regenerative reheated cycle solves the problem of low net specific work encountered in the regenerative cycle and it had high efficiency and a better power to weight ratio [11,12].

Furthermore, turbogenerators have a bug that stands out during the startup phase. The shaft inertia leads to an electric energy consumption delivered by the starter, and the heat-up time of the heat exchanger leads to an addition of fuel consumption that decreases with the increase of the heat exchanger outlet temperature. Those factors must be taken into consideration when computing the turbogenerator's overall efficiency. Recent work by Bou Nader et al. (2020) on Dymola software [12] studied the intercooled regenerative reheated cycle configuration where they took into consideration the startup and transient phase in their dynamic modeling [12]. Nevertheless, none of the previous studies has compared the performance of the different types of turbogenerators at the startup phase. This comparison will highlight the best energy converter candidate in the SHEV while taking into account the dynamic behavior of the system.

Based on these findings, and to select the best turbogenerator in automotive applications, this paper proposes dynamic modeling of different turbogenerator configurations for SHEV to evaluate the fuel consumption penalty during the transient startup phase. The methodology adopted in this paper provides advice and instructions for the design of highly efficient turbines, compressors, and heat exchangers, by reducing energy losses through these components, thus obtaining optimum turbogenerator configurations. It could be expanded and applied to reproduce new types of turbogenerator energy architectures and simulate them to compare their performances and select the best designs. The methodology steps are presented in section "Methodology", start from theoretical calculation to components design procedures to systems modelization and end with the turbogenerator's simulations. For each of the considered configurations, thermodynamic calculations were made to compute the overall efficiency and the net specific work while considering the component specifications. Based on the data of the thermodynamics studies, the operating conditions were defined and the turbomachines were designed on Ansys Vista. Then, a pre-design of the recuperators was made to calculate the weight and volume of the recuperator of each configuration. Thereafter, the different turbogenerator systems were modeled and simulated on Amesim. The Optimization process is proposed in every step of the methodology. First, in the thermodynamics study with variable compressing and expansion ratios and an objective of overall optimum efficiency. Second, in the turbomachines design with impellers geometry variation and an objective of highest attainable efficiency. Third, in the Amesim model operation with variable rotational speed and an objective of optimum rotational speed efficiency. The optimizations take into account the operations and manufacturing constraints of the system's components.

This study is novel in two ways. First, it presents a high-efficiency design procedure of each component for every single turbogenerator thermodynamic architecture, compressors, turbines, heat exchangers to get optimum turbogenerator's systems. Second, it is the first study that presents a dynamic performance comparison between the different possible turbogenerators for automotive application by considering the rotating machine's inertia and the heat exchanger thermal inertia impacts on fuel consumption, system efficiency, and temperatures during the startup phase.

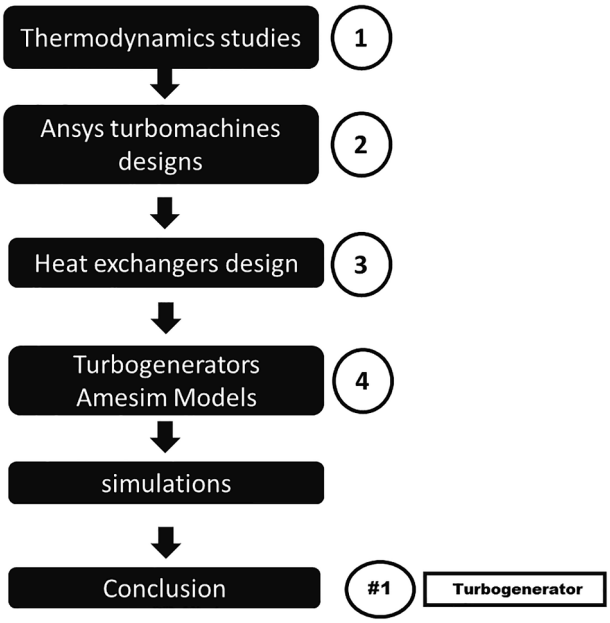

Fig. 2. Work methodology steps.

2. Methodology

This section presents the methodology adopted to compare the dynamic behavior that includes a comparison of the fuel consumption and the combustion chamber inlet temperature variation of the turbogenerators at the startup phase. The method consists of a four-step assessment plan as presented in Fig. 2. The first assessment step consists of a thermodynamic analysis applied on different realistic turbogenerators configurations identified in paper [9] and presented in Fig. 3, where the system efficiency and the net specific work were calculated. The technological and operational limitations of the components, for example, the maximum compression ratio of compressors, the maximum expansion rate of the turbine, and the maximum efficiency of the components were taken into account. These specifications are based on the most recent available component data. In the second assessment step, the different turbogenerators' turbomachines were designed on Ansys. The design data, inlet temperature, pressure, compression ratio, expansion ratio, and mass flow rate were taken from the first assessment step. The design process sought highly efficient turbines and compressors where the losses of these machines were minimized by referring to both, losses correlations and CFD simulations.

In the third assessment step, the regenerators of the turbogenerators were designed, their mass and volume were computed to make a comparison between the different heat exchangers.

In the fourth assessment step, a dynamic model of each turbogenerator configuration was developed on Amesim and the data of the second and the third assessment, turbomachines maps, and heat exchanger specifications, were integrated into the models. The impact of the heat exchanger heat-up time on the efficiency and temperature, during the start-up phase, was evaluated by considering a constant start-up power strategy where higher fuel consumption is injected during the start-up to maintain the same turbogenerator output power. Also, a comparison in terms of fuel consumption and combustion chamber inlet temperature is done between the four turbogenerator systems.

Finally, the turbogenerator's efficiencies were evaluated on a battery charging duration. The comparison between the turbogenerator's startup dynamic performance and their efficiencies led to the selection of the best energy converter.

3. Thermodynamic analysis

This section presents the thermodynamics analysis of realistic turbogenerator systems presented in Fig. 3 to compute their efficiencies and net-specific work. The different turbogenerators investigated are: The simple cycle GT (A) consists of a compressor, a combustion chamber (CC), and a turbine and it works on a Brayton cycle principle. The regenerative cycle RGT (B) had a regenerator to benefit from gas exhaust temperature and preheat the inlet air of the combustion chamber. The compression is accomplished in two compressors with an intermediate intercooler in the intercooled regenerative cycle IRGT (C) to reduce the high-pressure compression stage inlet air temperature and so decrease its consumed power. The intercooled reheated regenerative cycle IRReGT (D) consists of two-stage intercooled centrifugal compressors, a regenerator, a two-stage reheat centrifugal turbines, and two

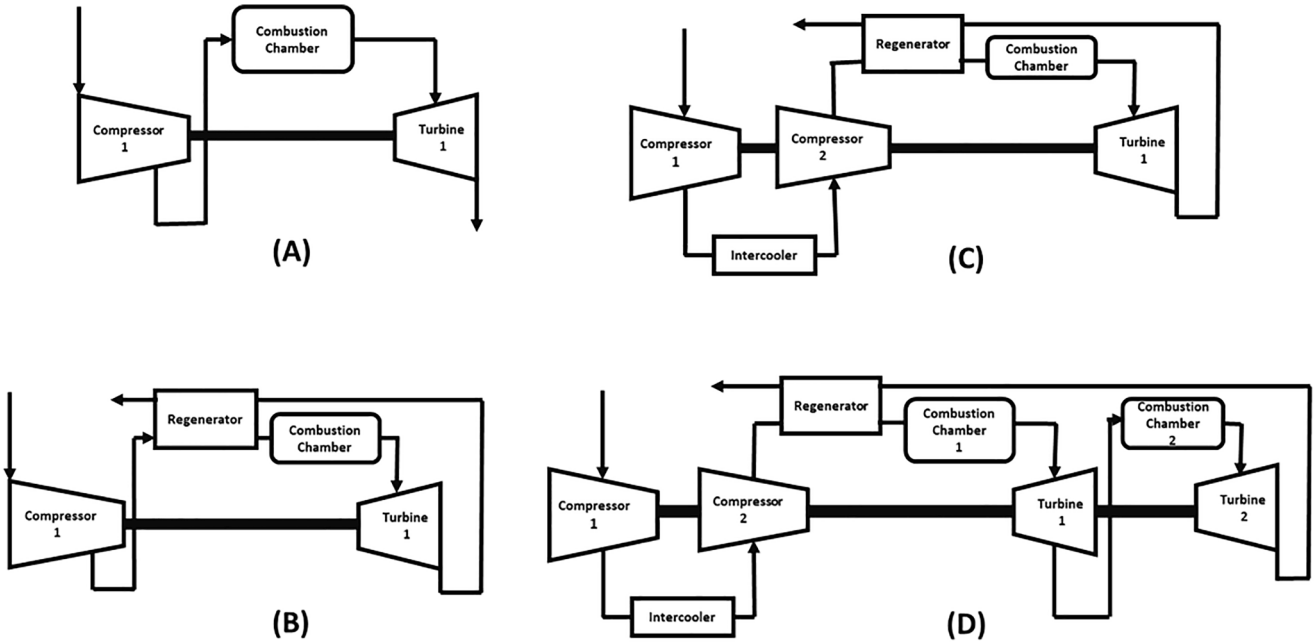

Fig. 3. The different configurations of the investigated turbogenerator systems: (A) GT, (B) RGT, (C) IRGT, and (D) IRReGT.

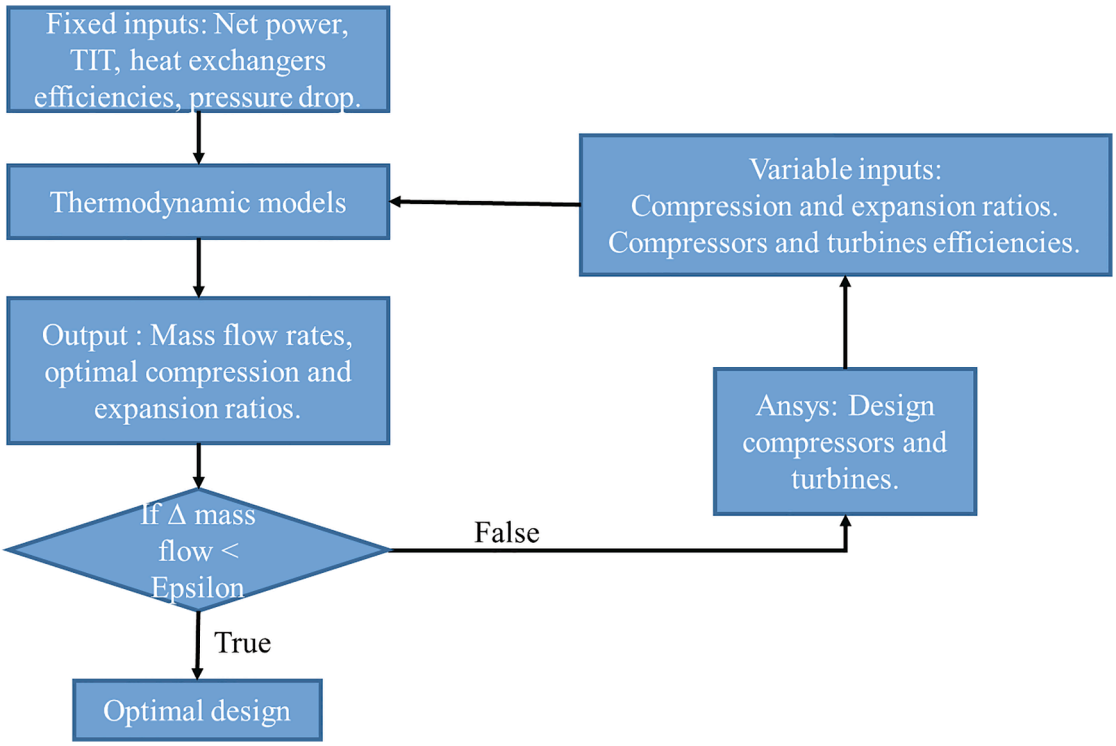

Fig. 4. Turbogenerators design loop.

combustion chambers. The air compressed in the low-pressure (LP) compressor stage is cooled by an intercooler before entering the high-pressure (HP) compressor stage. High-pressure air gains heat in the regenerator and enters at high temperature the first combustion chamber to gain heat again then make the first expansion in the high-pressure turbine stage. The gas is reheated in a second combustion chamber to expand again in the low-pressure turbine stage. Before leaving the system the gas exchange heat with the air.

The four types of turbogenerators were modeled on REFPROP using fixed and variable inputs as presented in Fig. 4. Fixed inputs were chosen as follows: Radial turbines are more performant with high inlet air temperature, but the maximum turbine inlet temperature TIT was limited to 950 °C to reduce the NOx emissions that occur at high temperatures and to use low-cost turbine materials in order reduce the prices of the turbogenerator. For a fair comparison between the turbogenerators' performances, we managed to use the same recuperator's efficiency in all turbogenerators. 25 kW for the turbogenerators net power, this amount of power is a necessary one to charge the battery of the Series hybrid electric vehicle while maintaining a constant state of charge (SOC) during constant speed high way driving [12]. Meanwhile, the variable inputs were obtained from the Ansys Vista turbomachines design. In the thermodynamic analysis, an optimization was made in terms of the best combination of compression and expansion ratios. The thermodynamics analysis output was used as inputs for Ansys to redesign the turbomachines with higher efficiencies, then the Ansys output values were used as the new variable inputs for the thermodynamic models. The optimal turbomachines design and operating conditions that lead to the highest turbogenerators' attainable efficiencies are obtained when the thermodynamic models' output converge.

The compressor and the turbine steady-state work are determined using equations (1) and (2)

(1) $W_{compressor} = hc_{outlet}\text{-}hc_{inlet}$
(2) $W_{turbine} = hT_{inlet}\text{-}hT_{outlet}$

Where $W_{compressor}$ is the compressor specific work (kJ/kg), hc_{outlet} is the specific enthalpy at compressor outlet (kJ/kg), hc_{inlet} is the specific enthalpy at compressor inlet (kJ/kg), $W_{turbine}$ is the turbine specific work (kJ/kg), hT_{outlet} is the specific enthalpy at turbine outlet (kJ/kg), and hT_{inlet} is the specific enthalpy at turbine inlet (kJ/kg). The heat added in the combustion chamber (Q_{CC}) is computed using equation (3).

(3) $Q_{CC} = hCC_{outlet} - hCC_{inlet}$

The system energy efficiency (η_{system}) is computed according to equation (4).

(4) $\eta_{system} = \frac{WTurbine - WCompressor}{Qcc} = \frac{Wnet}{Qcc}$

Where W_{net} is the system net specific work (kJ/kg).
The air mass flow rate in the cycle is computed using equation (5).

(5) $m_{air} = \frac{P_{net}}{W_{net}}$

Where P_{net} is the system net power that the turbogenerator must deliver.

4. Turbomachines design

The efficiency of the turbogenerator relies on its components efficiencies, from this point we decided to make studies about designing high efficiencies turbomachines since the maps of these turbomachines will be integrated into the turbogenerators Amesim models for simulations. The turbomachines study consists of three steps. Starting with a general theoretical approach about centrifugal compressors and radial turbines to better understand what parameters have the biggest impact on efficiency, then the design and the improvement were done with Ansys (vista CCD, Vista RTD) and turbomachinery fluid flow for CFD simulations. The highest attainable efficiency is possible by choosing the optimum rotation speed design point and the optimum impeller geometry basing on losses correlations. Finally, in the last step, the

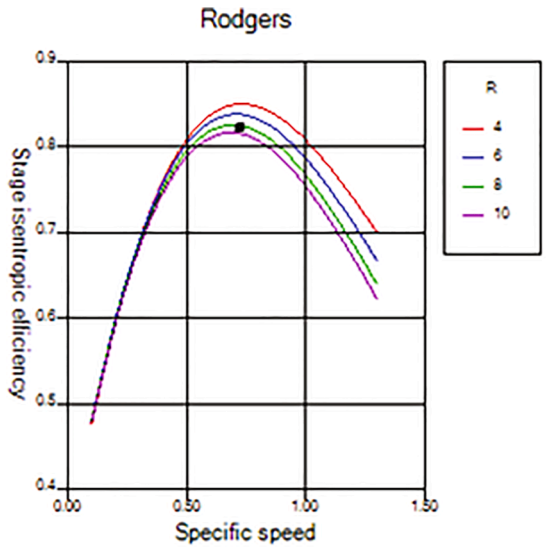

Fig. 5. Rodgers charts showing the variation of the compressor isentropic efficiency depending on its specific speed.

turbomachines maps were generated.

4.1. Centrifugal compressor design

This section presents the centrifugal compressor design study. Centrifugal compressor performance was examined analytically to determine optimum geometry as characterized by specific speed. For the desired duty many combinations of velocity diagram characteristics and compressor geometric parameters are possible. The combinations of greatest interest are those that will result in maximum attainable efficiency.

In the design procedure of a centrifugal compressor, the choice of an optimum rotational speed design point is important, because this rotational speed will define the value of the specific speed of the compressor, and the losses are related to the specific speed. To minimize the losses, the specific speed which is a term that relates compressor rotational speed, flow rate, and ideal enthalpy rise must be in the optimum zone. Impellers associated with a large total head and low flow rate are characterized by low specific speed and, conversely, those with a low total head and high flow rate are characterized by a high specific speed [13]. The choice of the rotational speed design point optimal value was based on the Rodgers chart (Fig. 5) to get an optimum specific speed value where the highest efficiency occurs. The correlation of Rodgers presented the relation of specific speed and efficiency, it suggests that an optimum specific speed Ns exists for a given stage pressure ratio. This relation showed that at a low specific speed, efficiency drops due to an increase in the frictional losses in the vane passages and the disc friction. However, at a high specific speed, efficiency drops due to an increase in the aerodynamic losses resulted from the high relative velocity levels [15]. The specific speed expression is defined as follow $Ns = \frac{\Omega \cdot \sqrt{Q_1}}{(\Delta H_0)^{\frac{3}{4}}}$. The maximum attainable efficiency corresponds to a specific speed near 0.7.

Moreover, to design the optimum geometry that leads to the highest attainable efficiency, the study based on ANSYS Vista CCD, on Rodgers chart relying on the losses correlations. From losses formulas, it was found that the impeller blade exit angle (ßb2 encircled in green- Fig. 6) and the exit to the inlet relative velocity ratio (W2/W1 encircled in red- Fig. 6) have a major effect on losses and those parameters define the impeller geometry, dimensions, and angles.

Therefore, seven specific losses were evaluated for various combinations of the exit to the inlet relative velocity ratio and the blade exit angle. The losses considered were the incidence loss, blade loading loss, skin friction loss, disk friction loss, clearance loss, recirculation loss, and the vanned and unvanned diffuser loss. Incidence loss occurs at the inlet of the rotor and depends on the inlet Mach number and the leading edge geometry. The Blade loading loss is caused by the boundary-layer growth in the impeller and highly dependent on the internal diffusion (variation of the relative velocity) of the working fluid. The friction losses are one hand, the skin friction between the flow and the impeller blade surfaces, for reduction, smooth surfaces, low-velocity levels, and wide but not too long flow channels should be taken into consideration.

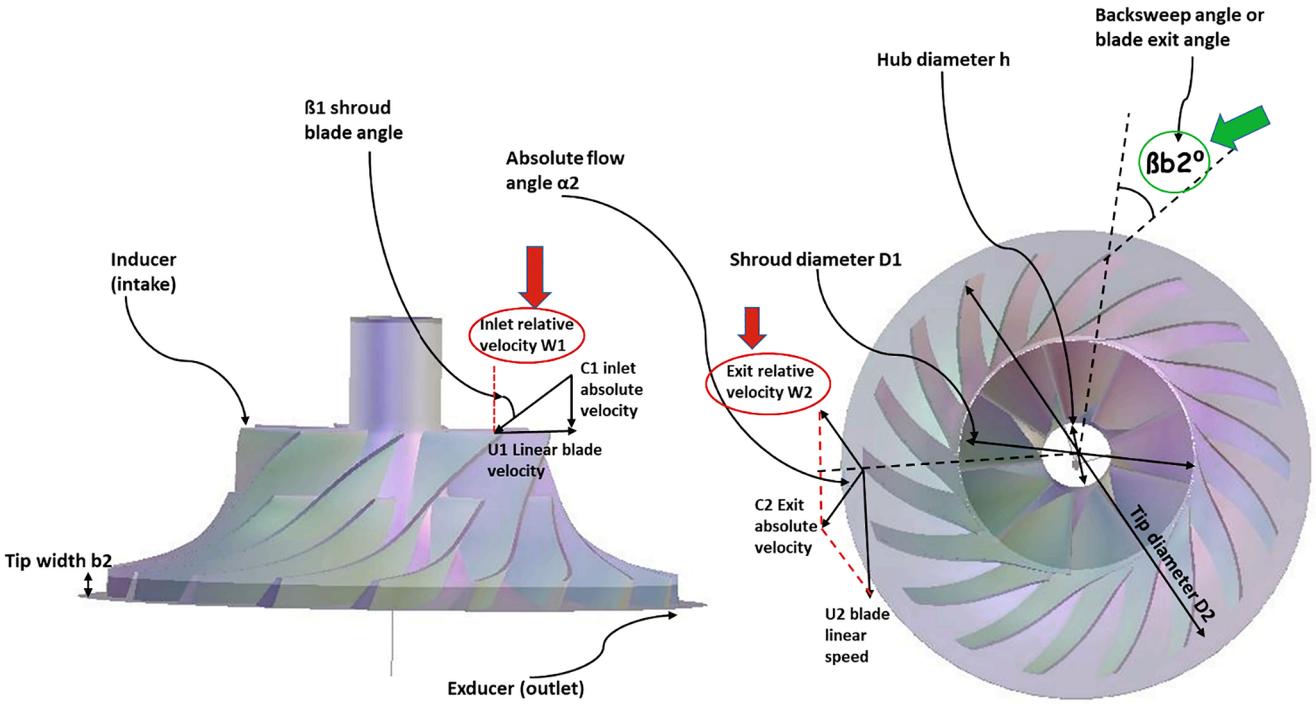

Fig. 6. Geometry and velocity triangle annotation for centrifugal compressor impeller.

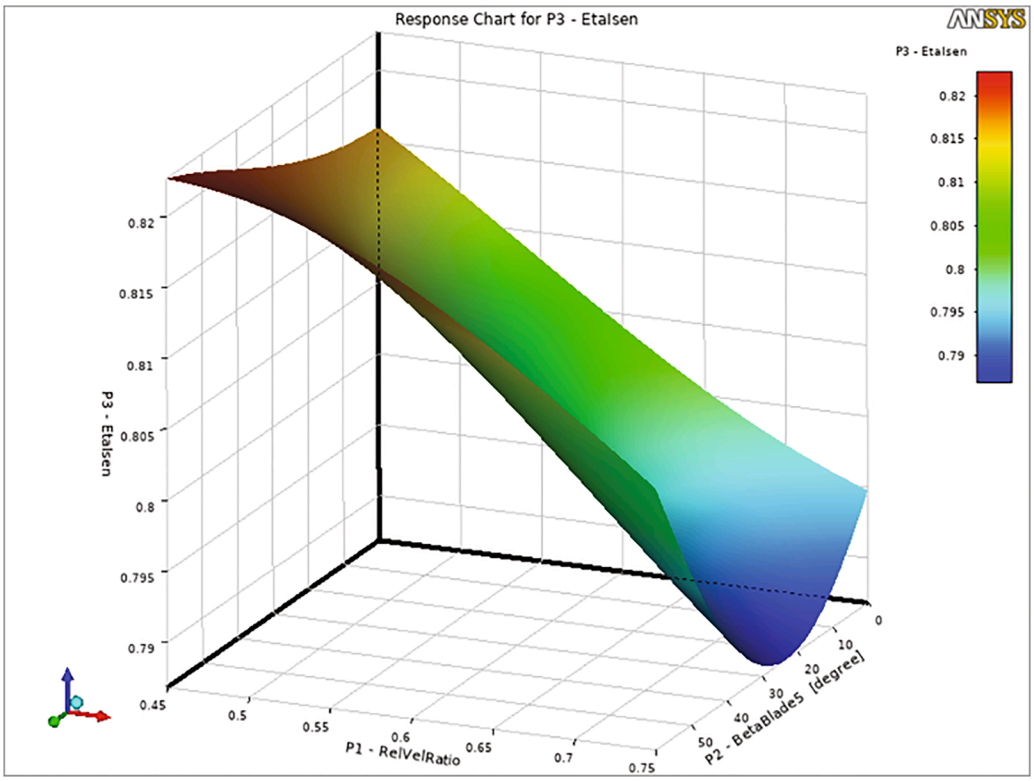

Fig. 7. Compressor stage isentropic efficiency evolution depending on the exit to inlet relative velocity ratio and the beta blade exit angle.

On the other hand, the disk friction caused by the fluid between the impeller shrouds (blade extremity) and the stator intern surface, this loss became minimal at a certain flow coefficient. Clearance loss happened due to the flow that occupies the gap between the rotor and the stator that doesn't participate in the energy transfer, the proportion of this flow decrease if the blade height increase, maximizing the ratio of the blade tip width over the radius of the exducer b2/R2 will minimize this loss. The Recirculation loss incurred through the additional work done on the working fluid due to back-flow from the vanned diffuser to the impeller and increases with a high absolute exit flow angle (α_2). Vaneless diffuser loss is a friction loss meanwhile vanned diffuser loss depends on Mach number at the inlet, blockage, area ratio, and pressure recovery. The vanless space is necessary for decreasing the velocity at the vanned part and reduce shock loss, for this reason, the Max Mach number at the vanned diffuser inlet should not exceed 0.8. [13,17,18]. The main losses are expressed in the five equations below [17]. The Formulas terms explanation are in appendix A symbols.

(6) $\Delta H_{cl} = 0{,}1.\ \frac{g}{b2}.U_2^2$

(7) $\Delta H_{df} = (C_{mi} + C_{md}).\rho_2.U_2^3.R_2^2/\ (2.m).$

(8) $\Delta H_{sf} = 5{,}6.\ Cf.\frac{Lb}{Dhyd}.C_{2m}^2$

(9) $\Delta H_{rl} = 0{,}02.\sqrt{\tan\alpha_2}\ .D_f^2.U_2^2.$

(10) $\Delta H_{bl} = 0{,}05\ .D_f^2.U_2^2$

(11) $D_f = \frac{W_2}{W_1} + \frac{0.75.\Delta H_0}{U_2^2} / (\frac{W_2}{W_1}.\frac{Z}{\pi}(1 - \frac{r_1}{r_2}) + \frac{2.r_1}{r_2})$

The variation of the geometry dimensions, the velocity triangles, and the compressor losses was evaluated according to the variation of the exit to the inlet relative velocity ratio and the blade exit angle separately referring to Ansys and losses correlation. While decreasing the exit to inlet relative velocity ratio we were decreasing the exducer diameter and the tip width was increasing to maintain the same compression ratio, resulting in losses reduction. The clearance loss decrease with increasing the tip width, because of the proportion of the flow that occupies the gap between the rotor and the stator that doesn't participate in the energy transfer decrease. The disk friction, the skin friction, the diffuser loss, the blade loading loss were also decreasing since they vary the same way, as the tip exit diameter and the blade tip exit linear speed. However, we noticed an increase in the recirculation losses because of an increase in exit absolute flow angle α_2

A backswept blade reduces the kinetic energy entering the diffuser thus reduces the diffuser losses and increases the stage efficiency, as a penalty, we increase the stress on the blade. After evaluating each loss variation according to the relative velocity ratio and the impeller blade exit angle, the response chart (Fig. 7) presents the compressor stage isentropic efficiency variation according to various combinations of these two parameters.

For a constant relative velocity ratio, the isentropic efficiency decreases when the blade exit angle increases from 0 to 25 degrees then it increases with higher blade angles. For a constant blade exit angle, the stage isentropic efficiency increases when the relative velocity ratio decreases, but below 0.5 it almost becomes constant. It was concluded that a low exit to the inlet relative velocity ratio coupled with a high exit blade angle is a very good way to improve the isentropic efficiency of the compressor stage and higher efficiency is expected with higher decelerating fluid through the rotor. Meanwhile, this improvement is accompanied by penalties thus constraints and limits. A high backsweep angle leads to high stresses on the blades and high-quality material must be used, Rodgers limit the relative velocity ratio because it causes a reduction in surge margin and the compressor risk to stall when working at different operating conditions, because of instantaneous high increase in flow separation from the blade surface [20].

Therefore, CFD simulations were done to check logical values of the temperatures, velocities, and Mach numbers through the designed impellers, then comparisons were made between two compressors designed for the same duty (pressure ratio and mass flow rate) to visualize the influence of the relative velocity ratio on the surge margin. The first one was designed for a relative velocity ratio of 0.5 and the second for 0.7 (Appendix B). Many simulations were done with different mass flow rates and rotation speeds, the flow separations through the passes

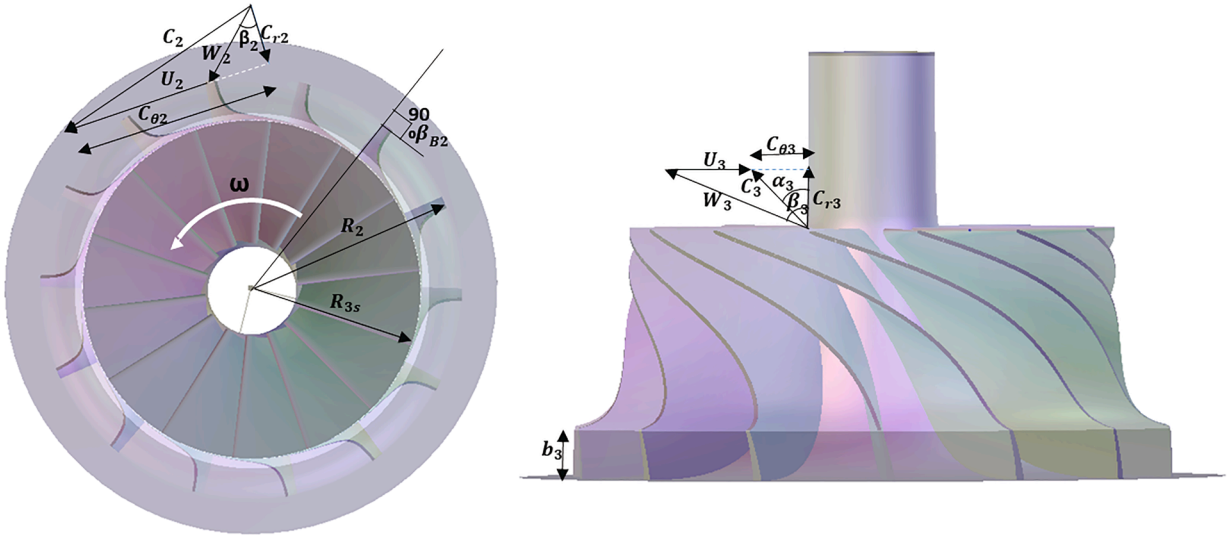

Fig. 8. Geometry and velocity triangle annotation for Radial turbine impeller.

of the two designed impellers happened at a lower mass flow rate and higher rotation speed in comparison to the compressor optimum design conditions.

From simulations (Figs. 17 and 18), no problems encountered in regions close to the hub and small local separation appears at the trailing edge of the mean radius zone in the impeller of a 0.5 relative velocity ratio. The major Surge margin reduction problems were manifested at the shroud side of the compressor with the low relative velocity ratio, where we could see high flow separation. For this reason, the minimum exit to the inlet relative velocity ratio was selected as 0.5 and the maximum blade exit angle was selected as 50°.

4.2. Radial turbine design

This section presents a radial turbine design study. Radial inflow turbines are suitable for a variety of applications in aircraft, space vehicles, and other systems where compact power sources are required. Designing a turbine for a specific duty is a choice of the best dimensions and angles combinations that give the required expansion ratio and mass flow rate at a specific speed with minimum losses. Changing any parameter resulting in a must of change of other parameters for duty conservation. We can reduce a specific loss by changing a specific parameter but since other parameters are changing at the same time, we must check the evolution of other losses that may be increasing or decreasing but there is always an optimum parameters combination (Fig. 8).

Seven specific losses were considered in the design. The friction loss depends on the geometry, velocities, friction coefficient of the components, and occurs through the Nozzle, rotor, and diffuser. The Loading loss occurs due to the aerodynamics loss of the flow and passage loss affected by the incidence angle and the geometry. The separation loss, which is the separation of the flow from the blade surface due to the high relative velocity ratio. Shock or incidence loss occurs at the leading edge of the rotor due to the difference between the flow angle and the optimum one. The clearance loss depends on the part of the flow in the gap between the rotor and stator that does not participate in the energy transfer with blades. Too tight air section passage leads to blockage loss at the nozzle and rotor trailing edge. The last loss is the exit kinetic loss caused by a high exhaust gas velocity. [14]

Moreover, maximum static efficiency and maximum total efficiency are expected for a specific speed Ns = 0.6 and Ns = 0.93 respectively [14], where the specific speed is a dimensionless number that relates to the rotation speed, the volume flow rate, and the ideal enthalpy drop. It expressed by $Ns = \frac{N.\sqrt{Q_2}}{(\Delta H_0)^{3/4}}$. High friction losses occur at a low specific speed, meanwhile, at a high specific speed, high kinetic loss occurs.

The study started by making a list of recommendations for the design and with ANSYS radial turbine design Vista RTD and Chen and Baines turbine efficiency map, losses were minimized with an optimum impeller geometry.

The radial turbine consists of 3 components, the nozzle, the impeller, and the diffuser. High-pressure gas enters the nozzle, as the geometry is divergent there is an energy transformation from potential to kinetic so the pressure of the flow decrease, and its velocity increase. The nozzle blade leads the flow with a specific exit flow angle adapted with the desired relative flow angle at the inlet of the rotorβ_2. An energy transfer from the flow (kinetic) to the blade (mechanic) occurs in the rotor, at the same time there is energy transformation from potential to kinetic. A divergent exhaust diffuser is used to decrease the exit velocity and transform a part of it to static pressure. The Specific work of the radial turbine is given by Euler relation: $W = C_{\theta 2}U_2 - C_{\theta 3}U_3$

Design recommendations were collected from the literature and presented below as a design reference [14,16], and [19]. Many losses occur due to high velocities like friction and exit kinetic energy which is proportional to the square of velocity for this reason very high velocities must be avoided. The inlet blade angle is selected as $ß_{B2} = 90°$ due to strength limitations, this angle is different from the flow relative velocity angle $ß_2$. Some designers will go for an inlet relative flow angle equal to zero ($ß_2 = 0$) and an axial absolute velocity ($\alpha_3 = 0$, $C_{\theta 3} = 0$) with a small magnitude to minimize kinetic energy loss, so $W = U_2^2$ and they increase U_2 with a limit concerning material and temperature constraints.

Whoever, in reality, best efficiencies and high specific work occur when the flow enters with negative incidence $ß_2 < 0$ (do not match the blade angle because blade loading leads to a good static pressure gradient and permits a good transformation of the energy from potential to kinetic). Moreover, a negative absolute angle α_3 is beneficial to increase the specific work ($C_{\theta 3} < 0$), referenced on the Euler equation, and the efficiency increase. Therefore, for the design, an optimum range of $ß_2$ is $-40° < ß_2 < -20°$, and $-30°$ is a good choice. A very high negative $ß_2$ angle will increase the losses (incidence loss or shock loss) even if it is better for blade loading. For the impeller exit absolute angle α_3, we designed the impeller to get an angle close to $-15°$, with a higher negative value, efficiency decreases fast with exit loss. For the impeller exit relative angle $ß_3$, minimizing Mach relative will minimize the internal passage losses and $ß_3 = -55°$ would be a good choice. Moreover, minimizing Mach absolute will minimize kinetic energy loss and $ß_3 =$

Table 1
Designed turbomachines data, mass flow rates, compression ratios, expansion ratios, and rotational speeds.

Turbogenerators 25 kW	GT	RGT	IRGT	IRReGT
Mass flow rate kg/s	0.162	0.189	0.163	0.122
π1	4	2.8	2.116	2.483
π2	–	–	1.598	1.871
τ1	4	2.8	3.381	2.841
τ2	–	–	–	1.635
RPM	130,000	100,000	80,000	90000/140000
η_{is} LP compressor 1	0.815	0.826	0.827	0.819
η_{is} HP compressor 2	–	–	0.829	0.818
η_{is} HP turbine 1	0.781	0.779	0.782	0.770
η_{is} LP turbine 2	–	–	–	0.768

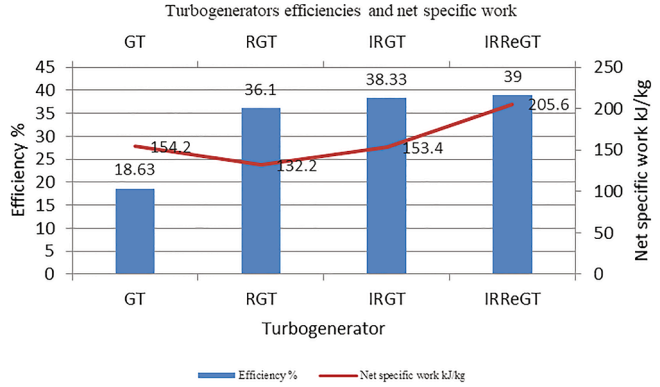

Fig. 9. Turbogenerators' efficiencies and Net-specific work.

−70° would be a good choice. Therefore, an optimum exit relative flow angle is defined as follows −70°< ß3 < −50°. In our design, we tried to be close to $ß_3 = -60°$, blockage, and high-stress levels should be considered with high $ß_3$. For reducing internal passage loss an optimal relative velocity ratio $\frac{w_3}{w_2} = 2$ and $\frac{w_{3s}}{w_2} = 2.5$ is recommended. Moreover, an increase in relative velocity ratio and relative velocity flow angle will lead to an increase in non-dimensional parameters like: $\frac{R3s}{R2}$ and $\frac{b3}{R2}$ and this lead to a decrease in both passage friction and clearance loss but the kinetic energy loss increase. A reduction of the ratio $\frac{w_2}{U_2}$ reduce stage losses. An optimum blade speed ratio: $\frac{U2}{Cs}$ will be between 0.6 and 0.7. With Cs the isentropic velocity or the spouting velocity, the velocity that would be obtained if the gas was expanded isentropically from the inlet stagnation enthalpy to the exit static condition, given by $C = \sqrt{2.\Delta his}$ where $\Delta his = H_{02}\text{-}H_3$. There is an optimum impeller inlet Mach number for any given power ratio Sw and inlet relative flow angle where $Sw = \frac{W}{m.h_{01}} = 1\text{-}\frac{T_{03}}{T_{01}}$, this range is between 0.5 and 0.7. With the same Mach number, the power ratio increase with increasing $ß_2$ negatively so it leads to an increase in specific work. The blade number was calculated using the formula from [19] $Z = \frac{\pi*(110-\alpha 2)*\tan\alpha 2}{30}$. Referring to Chen and Baines [21], maximum efficiency occurs for flow coefficients in the range 0.2–0.3, and at loading coefficients between about 0.8 and 1.With the loading coefficient: $\psi = \frac{\Delta h_0}{U_2^2}$ and Flow coefficient: $\Phi = \frac{Cr_2}{U_2}$, two dimensionless numbers that describe the stage performance. To these values corresponds an inlet absolute flow angle α_2 between 65° and 75°.

There are two critical points through the turbine where chock could occur, which is the point of maximum flow per unit area, and decrease the efficiency. Those points are the exit of the nozzle and the exit of the rotor. If the ratio of the absolute velocity over the critical speed (C_{cr}) at the nozzle exit is close to 1, we have a risk of chock, so the absolute angle at the nozzle exit α_2 must be changed, with $C_{cr} = \frac{\sqrt{2.k.R.T_0}}{k+1}$. If the ratio of the relative velocity over the critical speed at the rotor exit is close to 1 so there is a risk of chock, the relative flow angle $ß_3$ must be decreased.

Finally, with the turbomachines study we were able to design the radial machines of the four turbogenerators with the best combination of blade inlet and exit angles, diameters, and tip width that minimize the losses through the compressor and the turbine while taking into consideration the different manufacturing and performance constraints. After each design, the turbomachines maps were generated with ANSYS to integrate it into the AMESIM model later on for simulation.

The designed turbomachines data (mass flow rates, compression and expansion ratios, rotational speed, and isentropic efficiencies) are presented in Table 1. This table contains the optimal results of the loop in Fig. 4.

Each turbogenerator efficiency and net specific work came as mentioned below in Fig. 9.

At steady-state operation, the IRReGT had the highest efficiency among all turbogenerators. The interesting advantage of the IRReGT is that it fixed the low net specific work encountered in both RGT and IRGT turbogenerators so the IRReGT has a low air mass flow rate thus a reduced mass and size.

5. Recuperators design

This section presents the recuperators' design of the RGT, IRGT, and the IRReGT turbogenerators. A Gas-gas plate-fin heat exchanger (HEX) with counter-current flow was selected because of its compactness, reduced mass, and high attainable efficiency in comparison to other types of heat exchangers. For a fair HEX mass and volume comparison that leads to a fair comparison between the turbogenerators performances, we managed that the three recuperators have the same: efficiency 0,83, global heat exchange coefficient 151 W/m^2, fin efficiency 0.85, fin area to total area ratio 0.785, plate thickness 0.8 mm, and fin thickness 0.2 mm. The heat exchanger design is an iterative procedure presented in the HEX calculations procedure section, starting with an estimation of the heat exchange coefficient and aiming for a heat exchanger efficiency of 0.83. The design constraints were the heat exchanger dimensions and the maximum pressure losses that mainly depend on Renold's numbers, the hydraulic diameter, and the free flow sectional area.

HEX calculations procedure [22]:

(12)	$Nu = a*Re^{0.663}*Pr^{1/3}$	$0.087 < a < 0.4$
(13)	$Re = \frac{\rho*V*D_h}{\mu}$	$300 < Re < 4000$
(14)	$Pr = \frac{\mu*Cp}{\lambda}$	
(15)	$Nu = \frac{h*D_h}{\lambda}$	$30 < h < 300$
(16)	$D_h = \frac{4*A_o*L_1}{A_{fr}}$	
(17)	$X = \frac{A_o}{A_{fr}}$ $0.3 < X < 0.35$	
(18)	$\eta_0 = [\ 1\text{-}(1\text{-}\eta_f)*\frac{A_{fin}}{A}]$	$0.8 < \eta_f < 0.9$
(19)	$R_{conv} = \frac{1}{h*\eta_0}$	
(20)	$R_{plate} = \frac{e_{plate}}{k}$	
(21)	$R_{tot} = R_{conv,hot} + R_{wall} + R_{conv,cold}$	
(22)	$U = \frac{1}{R_{tot}}$	
(23)	$NTU = \frac{U*A}{C_{min}}$	
(24)	$A = A_{plate} + A_{fin}$	
(25)	$\sigma = \frac{A_{fin}}{A}$	$0.75 < \sigma < 0.85$
(26)	$A_{fr} = L_2*L_3$	
(27)	$HEX_{vol} = A_{fr}*L_1$	
(28)	$HEX_{mass} = \rho_{AISI347} * (A_{plate} * e_{plate} + A_{fin} * e_{fin})$	
	$0.5\ mm < e_{plate} < 1.2\ mm$;	$0.1\ mm < e_{fin} < 0.6\ mm$
(29)	$\varepsilon = \frac{1 - e^{-NTU.(1-C_{cr})}}{1 - C_{cr}.e^{-NTU.(1-C_{cr})}}$	$C_{cr} = \frac{C_{min}}{C_{max}}$ $C = m.C_p$
(30)	$q = \varepsilon.\ C_{min}.\ (T_{Hi}\text{-}T_{ci})$	

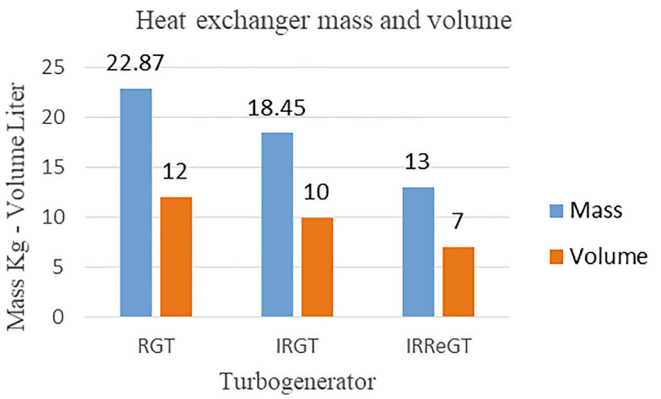

Fig. 10. Turbogenerator's heat exchanger mass and volume.

Where Re is the Renolds number, Pr the Prandtl number, V the flow velocity, m the mass flow rate, ρ is density and μ the kinematic viscosity of the fluid, D_h the hydraulic diameter (characteristic length), λ the fluid thermal conductivity, A_o the free flow cross-sectional area of the gas or the air, A_{fr} the heat exchanger frontal area, L_1 the heat exchanger length, L_2 heat exchanger height, L_3 heat exchanger width, A the total heat exchange area, A_{fin} the fin area, A_{plate} the plate area, η_{fin} the fin efficiency, η_o total exchange surface efficiency, h the convective exchange coefficient, k the heat exchanger material thermal conductivity, e_{plate} the plate thickness, e_{fin} fin thickness, R_{conv} the convective resistance at each side of the heat exchanger, R_{plate} the wall thermal resistance, U the global heat exchange coefficient, $\rho_{AISI347}$ the stainless steel density, ε the heat exchanger efficiency, q the flow heat exchange, HEX_{vol} the total volume of the heat exchanger and finally the HEX_{mass} is the heat exchanger total mass. AISI 347 stainless steel was used in the design.

After the design, the mass and the total volume of each HEX were computed. The Heat exchanger of the IRReGT had the smallest convective exchange area since the RGT and the IRGT are handling higher heat and mass flow rates (from thermodynamic analysis). Thus the recuperator of the IRReGT had the smallest size, and mass (Fig. 10). The heat exchanger data will be incorporated in the turbogenerator's dynamic models for simulation where the lag of the heat exchanger mainly depends on its mass and volume.

6. Turbogenerators dynamic modelization

This section presents the dynamic modeling of the turbogenerators on Amesim (The GT, RGT, IRGT, and the IRReGT) to study the inlet combustion chamber temperature variation and the fuel consumption of the machine. Then to compute the turbogenerators efficiencies taking into account the startup phase where the inertia of the components, mainly the turboshaft inertia and the heat exchanger heating time, has a big influence. The heat exchanger is heavy and cold at startup, it takes time to be heated and to give the required output temperature, so the turbogenerator can't reach its optimum efficiency rapidly, there is a startup transient phase characterized by an additional fuel consumption to countervail the inertia lag. From the solution of the Fourier-Biot equation (31), assuming one-dimensional heat transfer in the x-direction and constant thermal conductivity, we can obtain the temperature field of the heat exchanger intern wall as a function of time. Moreover, the solution of Newton equation (32) gives us the temperature variation of the heat exchanger at the startup phase.

$$(31)\ K.\frac{\partial^2 T}{\partial x^2} + q_v = \rho.C_p.\frac{\partial T}{\partial t}$$

$$(32)\ m.Cp.\frac{dT}{dt} = h.A.(T_{inf} - T)$$

Where K is the material conductivity ($W.m^{-1}.K^{-1}$), q_v is the rate at which energy is generated per unit volume of the medium ($W.m^{-3}$), ρ is the density ($kg.m^3$), and C_p is the specific heat capacity ($J.kg^{-1}.K^{-1}$), m is the mass of the heat exchanger (kg), A the total heat exchange area

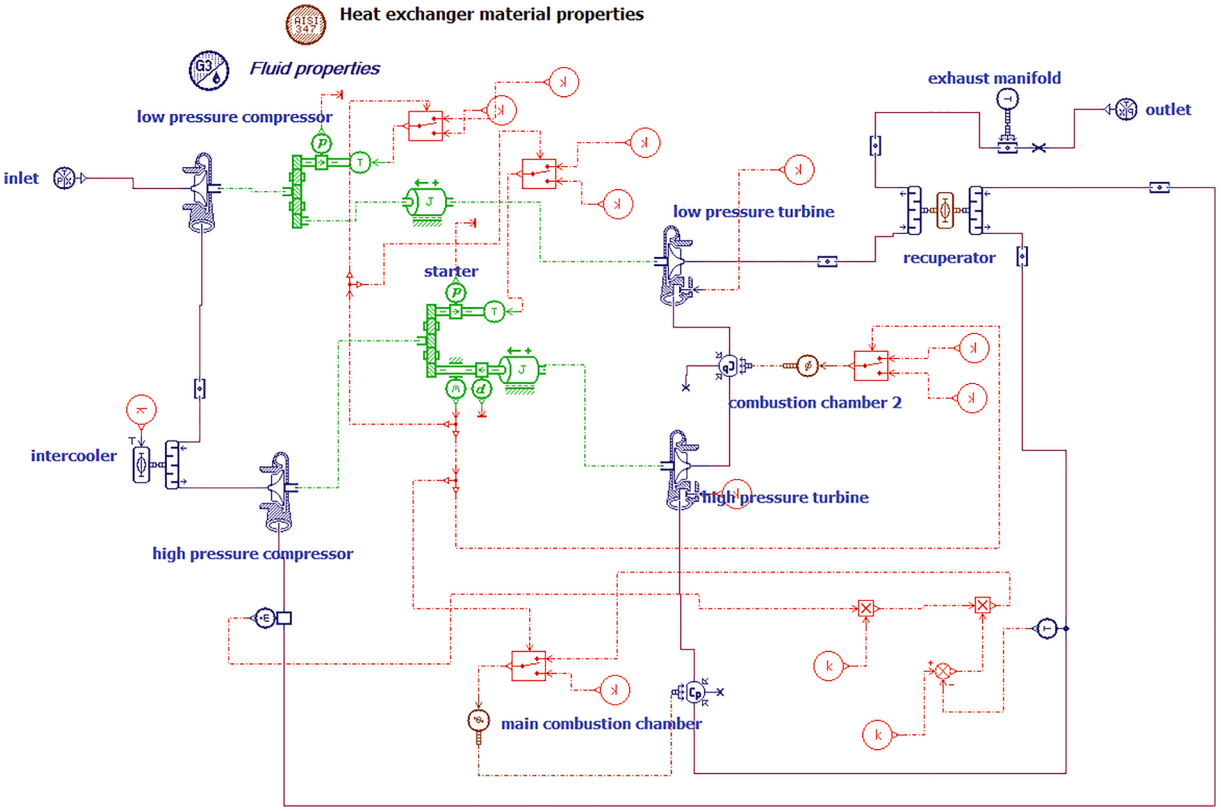

Fig. 11. IRReGT dynamic simulation on AMESim.

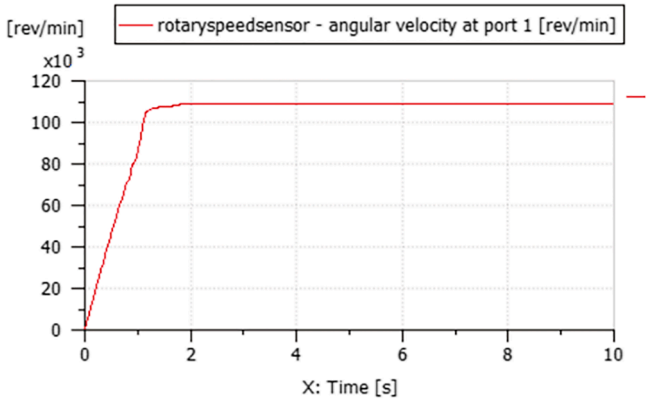

Fig. 12. RGT turboshaft acceleration at startup.

(m^2), h the convective heat exchange coefficient ($W.m^{-2}.K^{-1}$), t the time (seconds), T is the HEX temperature and T_{inf} is the HEX final exit temperature in kelvin.

The turbomachines maps generated in Ansys were extrapolated in Amesim and integrated into the models. The models were controlled to work at the optimum operating conditions of the turbomachines (rotation speed and mass flow rate). At low rotation speeds, the low air mass flow rate is not favorable for combustion. When reaching a specific rotation speed, the shaft speed sensor sends a signal to start the fuel injection at the CC, and at the same time, the starter is switched from motor to generator mode. The angular acceleration is obtained from equation (33), the first term presents the total moment inertia times the angular acceleration, and the second term presents the sum of the external torques acting on the shaft.

$$(33)\ J*\frac{d\omega}{dt} = \sum C_i = C_m + C_c + C_T + C_f$$

Where J is the system inertia including compressors, turbines, motor/generator, and shaft inertia ($kg.m^2$), dω/dt the angular acceleration (rad/s^2), C_i the sum of the torques (N.m), C_m the motor torque during starting (N.m), C_c the compressor torque (N.m), C_T the turbine torque (N.m), and C_f the friction torque (N.m). All ducts' lengths, diameters, and roughness take into consideration the pressure losses through the system. Both turbomachines and CCs were considered adiabatical with no heat exchange with the environment. Also, we assumed that the CC has no dynamic behavior, the temperature increase does not depend on the CC. The effect of these assumptions on the reliability of the result is very small. This must be proven through experiments. The first CC fuel injection was controlled according to the air mass flow rate and the CC inlet temperature, to have a constant CC exit temperature of 950 °C. The second CC in the case of the IRReGT has a constant fuel consumption since its inlet temperature is constant and independent from the recuperator exit temperature. The turbogenerators models operated close to the thermodynamic analysis values. Fig. 11 shows the IRReGT model on Amesim. The GT, the RGT, and the IRGT have similar but simpler models.

7. Results

This section presents the simulation results of the dynamic turbogenerators models. The simulations highlight three main comparisons at the startup phase. The first is a comparison between the impact of the recuperator and the starter on energy consumption. The second presents a comparison between the turbogenerators' fuel consumption and the combustion chamber inlet temperature. The last one presents the turbogenerator's efficiency comparison.

7.1. Recuperator and starter impact comparison at startup phase

The first simulation was to understand which part has the highest influence at the startup phase on fuel consumption. A 9 kW starter accelerates the turbomachines shaft from rest to nominal speed in<2 s (Fig. 12).

The recuperator lag was countervailed by an additional fuel consumption because the inlet combustion chamber temperature keeps increasing until the heat exchanger reaches a steady-state. So to obtain constant power from the turbogenerator we must inject more fuel at the

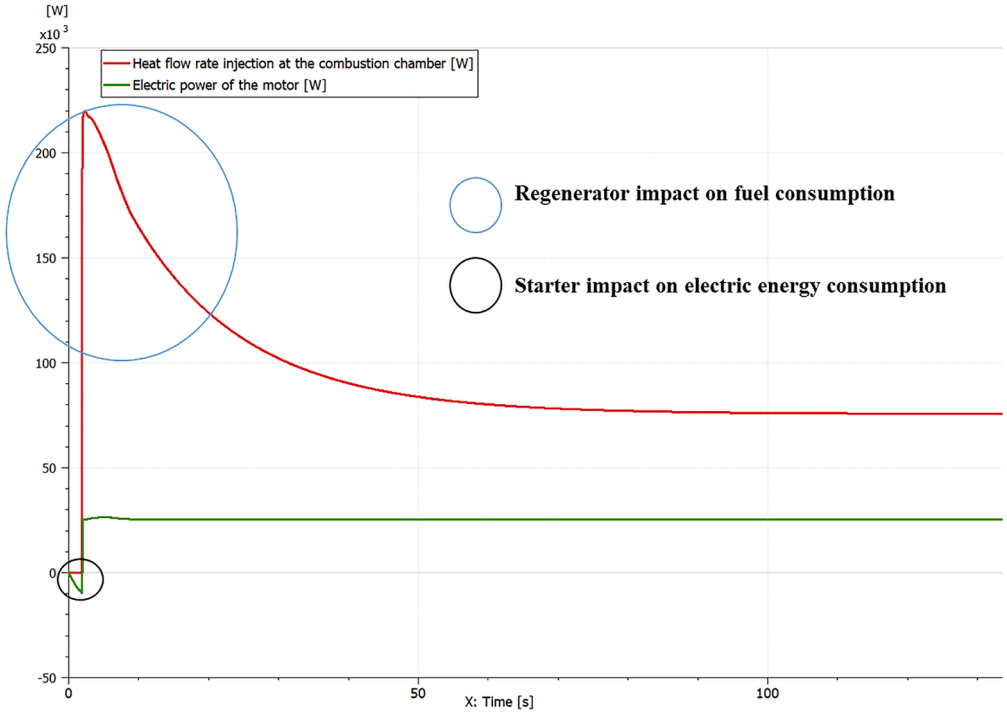

Fig. 13. Regenerator and starter impacts on additional energy consumption comparison at startup phase.

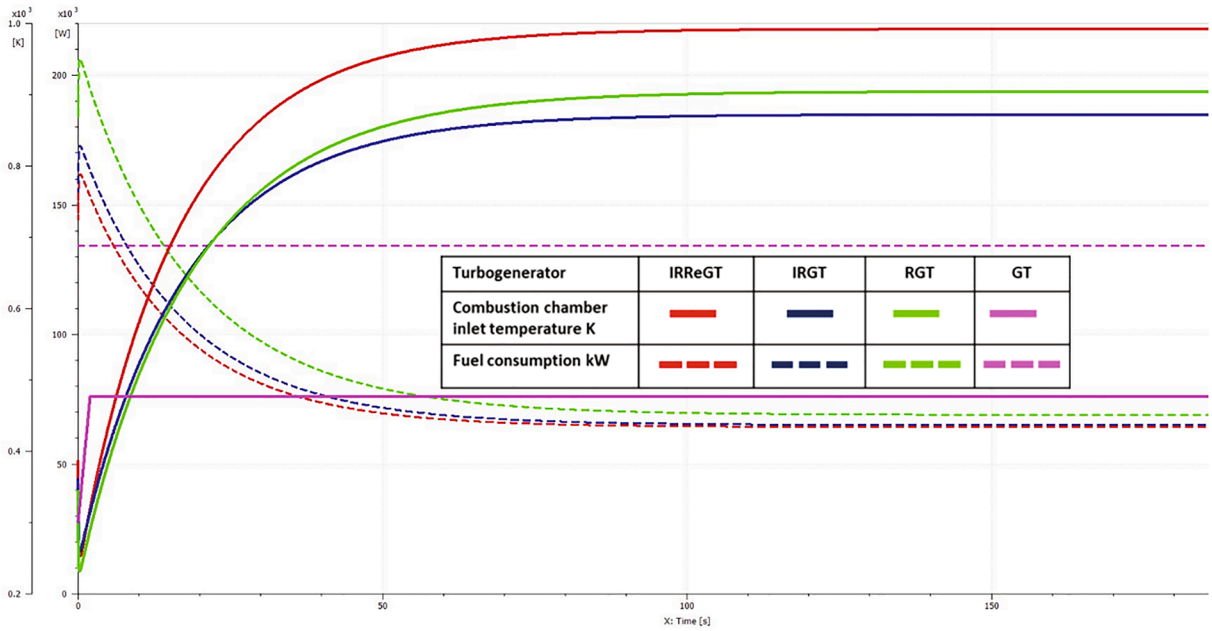

Fig. 14. The evolution of the IRReGT, IRGT, RGT, and the GT combustion chamber inlet temperature and fuel consumption at the startup phase.

startup phase.

Fig. 13 compares the starter and the recuperator impact on energy consumption at the startup phase, regenerative cycle simulation. The green line presents the power consumed by the E-motor (starter mode, a negative value) or generated (generator mode, positive value). The red line presents the fuel injection in kiloWatt at the combustion chamber. From the simulation, the impact of the starter on electric energy consumption is negligible in front of the recuperator's impact on fuel energy consumption.

The large difference between the impact of the recuperator and the starter on the additional energy consumption during the start-up phase is justified for two reasons. Firstly, the duration of the impact of the starter is very short (2 s) compared to that of the recuperator which is greater than 50 s, because the centrifugal turbomachines have small rotors and shaft masses. Second, the magnitude of the power between the recuperator and the starter. The turbogenerator only needs a 9 kW starter, meanwhile, the recuperator has a direct and huge impact on the amount of fuel injected into the combustion chamber which varies between a high range, 70 to 200 kW, due to the big difference between the inlet temperatures of the combustion chamber with (630 °C) and without recuperator (100 °C). Therefore, the next step is a study of the recuperator's influence on fuel consumption in the different types of turbogenerators and how much it reduces the turbogenerator efficiency. The 2 s acceleration time is ignored from this point.

7.2. Recuperator impact on fuel consumption and temperature

The second simulation (Fig. 14) focused on the rate of increase of the combustion chamber inlet temperature (continuous lines), resulting from the heat exchangers' behavior, and the addition of fuel consumption related to the variation of this temperature for the GT the RGT the IRGT and the IRReGT at the startup phase (Dashed lines).

The fuel consumption decreases when the combustion chamber inlet temperature increases with time. Because the role of the fuel injected in the combustion chamber is heating the gas to reach a specific temperature before expanding in the turbine, and the quantity of fuel injected is inversely proportional to the difference between the temperatures at the outlet and inlet of the combustion chamber according to the equation (34) $Q = m.Cp.(T_{out}-T_{in})$ where Q is the heat added to the gas, m the fuel mass flow rate, T_{in} and T_{out} are the combustion chamber inlet and outlet temperatures respectively. For the GT combustion chamber, the inlet temperature reaches its maximum in 2 s since there is no heat exchanger and depends only on the turbogenerator acceleration, this temperature rise is due to the compression of the air. But for the turbogenerators with recuperator (RGT, IRGT, and the IRReGT), the combustion chambers inlet temperatures reach their maximum after 70 s from the startup because of the inertia lag of the recuperator and the time that it needs to reach the steady-state. This duration depends on the final exit temperature of the recuperator, its mass, its volume or area, and its material-specific heat capacity according to the newton equation (32). While comparing the RGT with the IRGT we could see a close performance in temperature rise. Moreover, the rate of increase of IRReGT combustion chamber inlet temperature is higher than the RGT and the IRGT since it had the highest final exit temperature and the lowest recuperator mass which was obtained in the thermodynamic analysis and the heat exchangers calculation sections. The IRReGT HEX mass is 13 kg and its final exit temperature is 722 °C, meanwhile, the IRGT and the RGT masses are 18.45 kg and 22.87 kg, and their final temperatures are 633 °C and 601 °C, respectively. And according to equation (32), a lower HEX mass and higher HEX final temperature lead to a greater rate of temperature increase with time. Therefore the IRReGT fuel consumption stays lower than the other turbogenerators' consumption at all operation time, startup, and steady-state. However, the IRReGT recuperator's final output temperature is higher than the other turbogenerator's recuperators. Consequently, it took the IRReGT approximately the same time to reach the steady-state maximum efficiency in comparison with the RGT and the IRGT, even with a lower mass heat exchanger.

7.3. Turbogenerators efficiencies

In previous research [12], the powertrain of the series hybrid electric vehicle was adapted to medium-class hybrid vehicle performance. A 15 kW.h battery, charged by a 25 kW auxiliary power unit (the turbogenerator), provides the electricity to the E-motor. To compute new efficiencies that take into account the addition of fuel consumption at the startup phase, we make the third simulation on 1080 s which is the time needed to charge the 15 kW.h battery from 30% to 80% state of charge with a 25 kW turbogenerator.

From simulations (Fig. 15), the startup phase caused a reduction of 2.34% of the IRReGT efficiency (from 38,84% to 37,93%). This

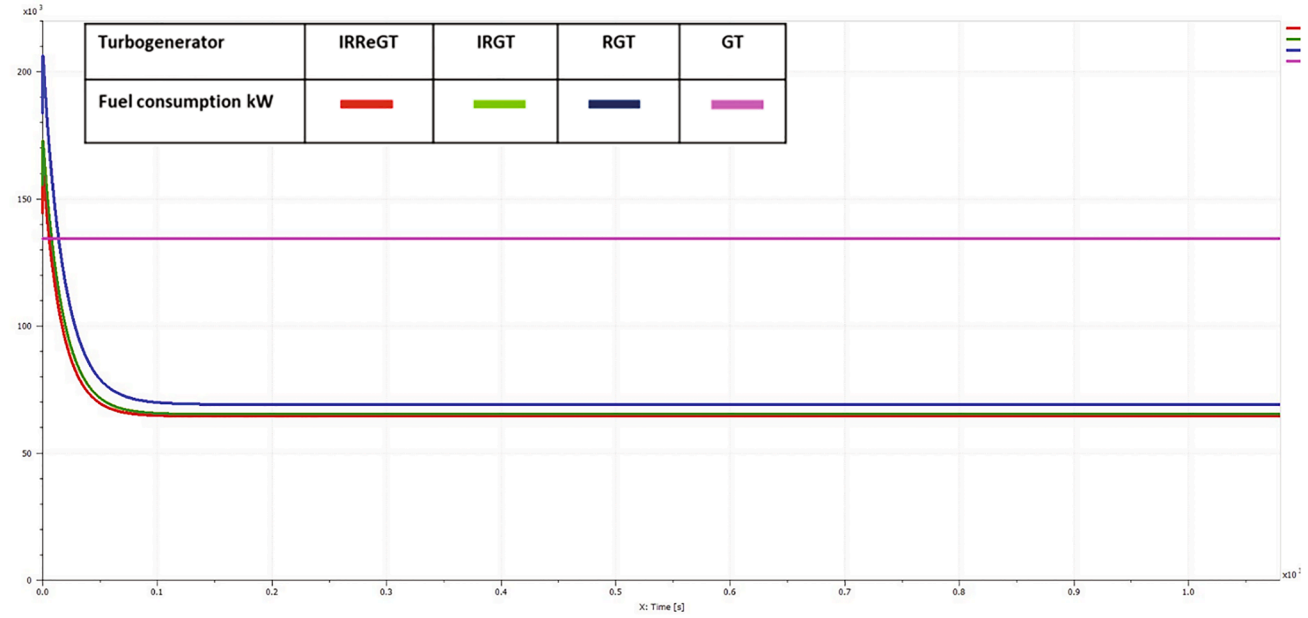

Fig. 15. Fuel consumption variation with time of the IRReGT, the IRGT, the RGT, and the GT.

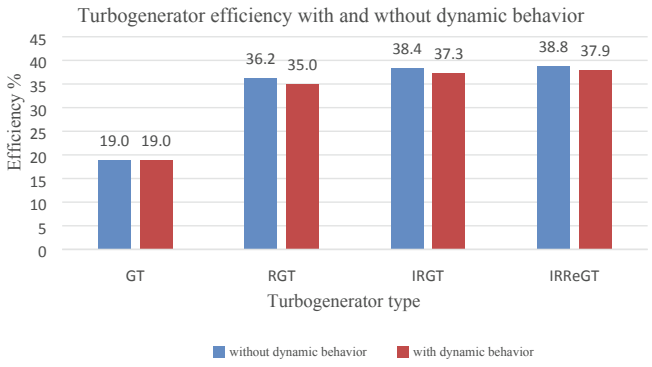

Fig. 16. Turbogenerators efficiency comparison with and without startup phase consideration.

reduction is 2.65% in the case of the IRGT (from 38.37% to 37.35%) and 3.4% in the case of the RGT (from 36.2% to 34.97%), so the startup phase has the biggest impact on efficiency in the RGT turbogenerator (Fig. 16). It is worth noting that the effect of the startup phase on efficiency becomes negligible if we consider one startup for a longer operation time. Moreover, a large number of startups will greatly reduce the efficiency of the turbogenerator. To verify the reliability of the new methodology presented in this article and then of the results obtained in the results section, several experimental tests are carried out. Heat exchangers, combustion chambers, and E-turbomachines have been manufactured and each component has been tested individually in steady-state as well as during transient start-up phases. The following steps aim to simulate a complete turbogenerator in its different configurations presented in this article. The experimental tests will be compared with the simulation results in a second article.

8. Conclusion

Turbogenerators present a forthcoming potential for integration as the main energy converter as the replacement of the internal combustion engine in series hybrid electric vehicle powertrain. A methodology was developed in this paper to study the performance of four different turbogenerators then to select the best one while taking into account the

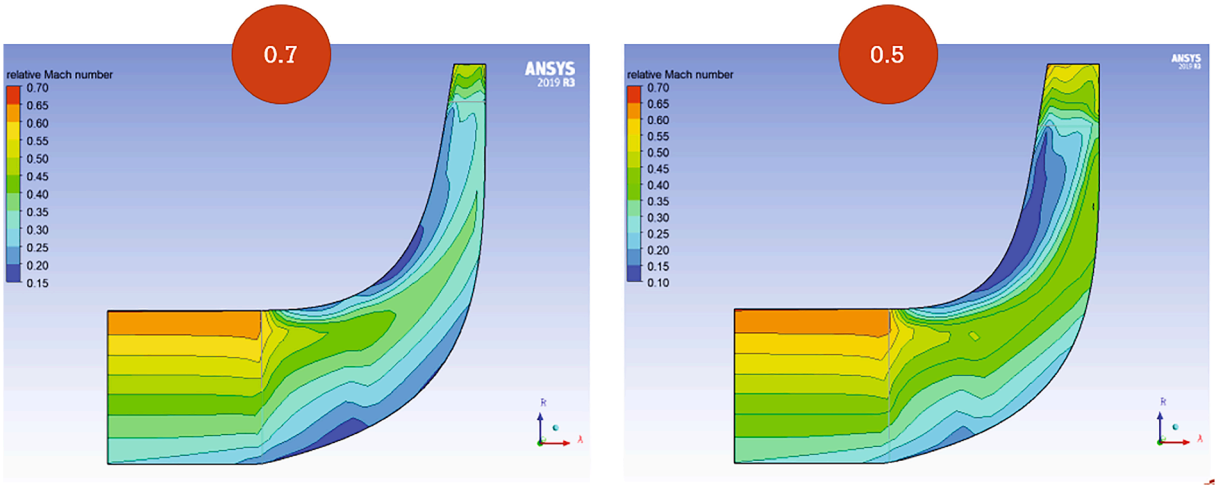

Fig. 17. Relative Mach number through the impellers of 0.5 and 0.7 relative velocity ratio designs.

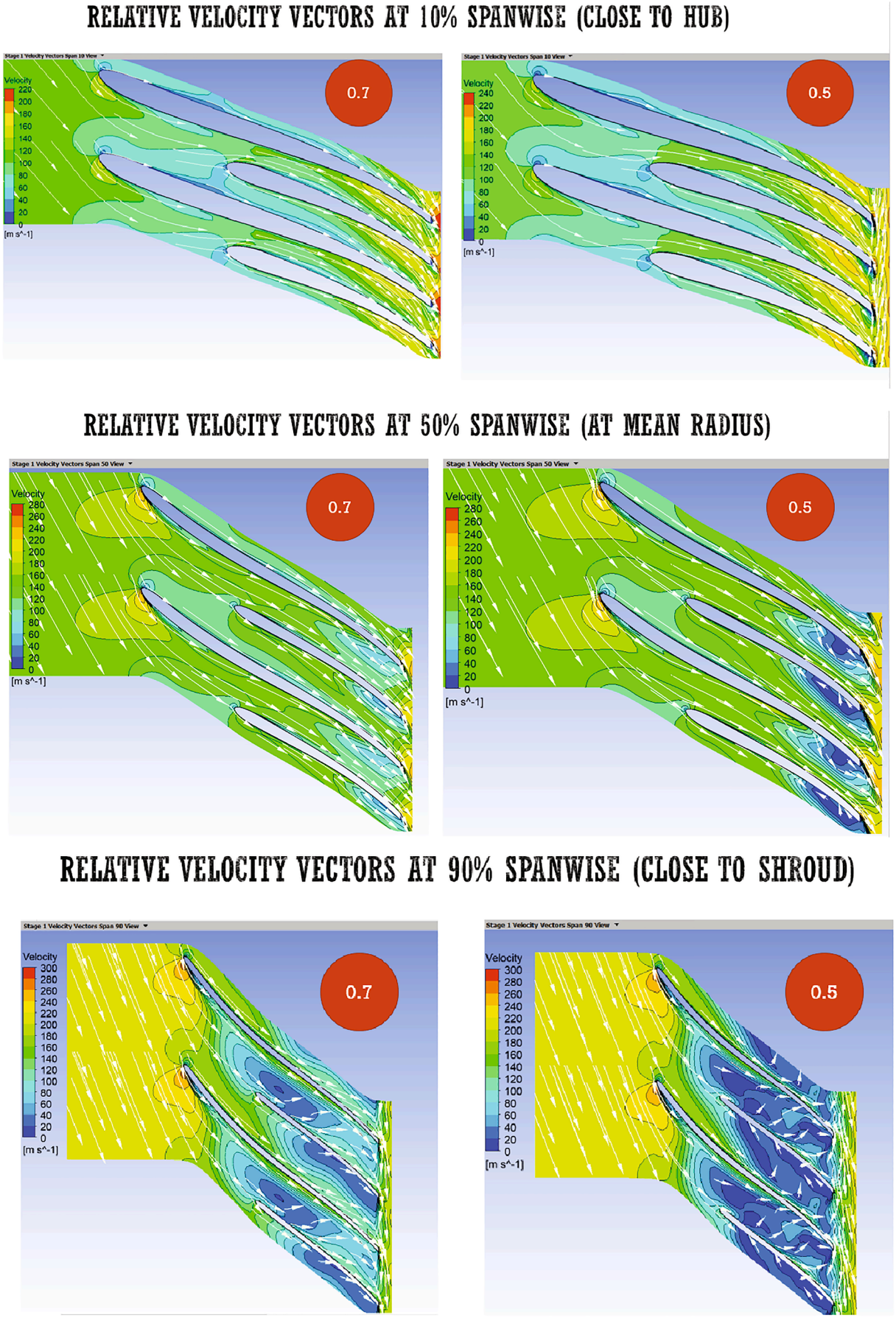

Fig. 18. Relative velocity vectors through the impellers of 0.5 and 0.7 relative velocity ratio designs.

system dynamic behavior. A thermodynamic analysis with optimization was made to evaluate the net specific work and the efficiency of each turbogenerator and to identify the components' optimum operating conditions. Then a design study based on the thermodynamic results was carried to design and generate the turbomachines maps of the different turbogenerators at high efficiency with optimum geometry parameters where the compressors and turbines losses were minimized, and to design the recuperators where their masses and volumes were computed. Thereafter, dynamic models of the turbogenerators were developed and simulated to evaluate and compare the fuel consumption and the combustion chambers inlet temperatures variation at the startup transient phase, also to compute the efficiencies of the investigated turbogenerators taking into account the dynamic behavior. Results show that the recuperator thermal inertia caused the main lag at the startup phase resulting in additional fuel consumption lasting for 70 s. Moreover, the intercooled reheated regenerative cycle IRReGT that consists of two-stage intercooled centrifugal compressors of 2.48 and 1.87 compression ratios for the low and high-pressure stages respectively, a recuperator, a two-stage reheat centrifugal turbines of 2.84 and 1.63 expansion ratios for the high and low-pressure stages respectively, and two combustion chambers, had the fastest response at the startup phase, the highest efficiency and net specific work of 37.9% and 205 kJ/kg respectively, for a turbine inlet temperature of 950 °C. A simple comparison between the efficiencies of the IRReGT as the best turbogenerator configuration with the SI-ICE of 36% efficiency operating as APUs in SHEV, shows that the turbogenerator presents a 5% fuel consumption reduction. Therefore, the intercooled reheated regenerative cycle was selected as the best candidate for replacing the internal combustion engine in the Series hybrid electric vehicle. After selecting the turbogenerator configuration, new research began to develop a complete vehicle model that combines the turbogenerator with the thermal power demand of the vehicle and improves its energy management by finding the best strategy to switch On/Off the turbogenerator. Also, the start-up phase will be improved to reduce emissions in order to comply with Euro 7 regulations on WLTP.

Thank you

The authors would like to thank the Groupe PSA.

Declaration of Competing Interest

The authors declare that they have no known competing financial interests or personal relationships that could have appeared to influence the work reported in this paper.

Appendix A

Symbols

SHEV	Series Hybrid Electric Vehicle
HEX	Heat Exchanger
ICE	Internal Combustion Engine
GT	Simple cycle gas turbine
RGT	Regenerative cycle.
IRGT	Intercooled Regenerative cycle.
IRReGT	Intercooled Reheated Regenerative cycle.
APU	Auxiliary Power Unit
SI-ICE	Spark Ignition Internal Combustion Engine
PEMFC	Polymer Electrolyte Membrane Fuel Cells
SOC	State Of Charge
TIT	Turbine Inlet Temperature
WLTP	Worldwide Harmonised Light Vehicles Test Procedure
CCD	Centrifugal Compressor Design
RTD	Radial Turbine Design
CFD	Computational Fluid Dynamics
HP	High Pressure
LP	Low Pressure
C	Absolute velocity, m/s
W	Relative velocity, m/s
U	Blade linear speed, m/s
C_u-C_θ	Absolute tangential velocity, m/s
C_m-C_r	Absolute meridional velocity, m/s
D	Diameter, m
R-r	Radius, m
b	Tip width, m
h	Hub diameter, m
α	Absolute flow angle, meridional, degree
ß	Relative flow angle, meridional, degree
$ß_b$	Backsweep, blade exit angle, degree
m	Mass flow rate, kg/s
Q	Volume flow rate, m^3/s
P	Pressure, N/m^2
T	Temperature, kelvin
ρ	Density, kg/m^3
R	Gas constant, J/(kg. K)
K	The ratio of specific heat at constant pressure to specific heat at constant volume
Ω	Radian rotation speed
N	Rotation speed rpm
Ns	Specific speed, dimensionless
η	Efficiency
τ	Expansion ratio
π	Compression ratio
ΔH	Incremental enthalpy through the rotor J/kg

(*continued on next page*)

(*continued*)

H	Enthalpy, J/kg
Ψ	Loading parameter, head coefficient
Φ	Flow coefficient
ΔH_{cl}	Clearance loss
ΔH_{df}	Disk friction loss
ΔH_{sf}	Skin friction loss
ΔH_{rl}	Recirculation loss
ΔH_{bl}	Blade loading loss
g	Clearance gap
Df	Diffusion factor
Cf	Skin friction coefficient
Lb	Impeller flow length
Dhyd	The impeller average hydraulic diameter.
M	Mach number
Z	Number of blades
Sw	Power ratio
Subscripts	
0	Total parameter
cr	Critical parameter
i	Impeller
d	Diffuser
1	Impeller inlet (compressor)/nozzle inlet (turbine)
2	Impeller outlet (compressor)/ impeller inlet (turbine)
3	Impeller outlet (turbine)
s	Shroud
t-t	Total to Total
t-s	Total to Static

B. CFD simulation

The dark blue area corresponds to the flow separation zone where the relative velocity and the relative Mach number are equal to zero. This area is located at the shroud side and it is larger in the impeller of 0.5 relative velocity ratio than the impeller of 0.7.

References

[1] https://ec.europa.eu/clima/policies/transport_en.
[2] https://ec.europa.eu/clima/policies/transport/vehicles/cars_en.
[3] Technical Information Engineering Office. History of Chrysler Corporation gas turbine vehicles. Report, Chrysler Corporation, Auburn Mills, MI, January 1979.
[4] Aya A. Barakat, Jad H. Diab, Nael S. Badawi, Wissam S. Bou Nader, Charbel J. Mansour Combined cycle gas turbine system optimization for extended range electric vehicles Energy Conversion and Management, 2020.https://doi.org/10.1016/j.enconman.2020.113538.
[5] Anon A. A light compact environmentally friendly powerplant. Sweden: Press Release for the VOLVO Environmental concept car (ECC); 1992.
[6] Cunha HE, Kyprianidis KG. Investigation of the potential of gas turbines for vehicular applications. Proceedings of the ASME Turbo Expo. 2012;3:51–64. https://doi.org/10.1115/GT2012-68402.
[7] Capata R, Coccia A, Lora M. A proposal for CO2 Abatement in urban areas: The UDR1-Lethe© turbo-hybrid vehicle. Energies. 2011;4(3):368–88. https://doi.org/10.3390/en4030368.
[8] Memon AG, Harijan K, Uqaili MA, Memon RA. Thermo-environmental and economic analysis of simple and regenerative gas turbine cycles with regression modeling and optimization. Energy Convers Manage 2013;76:852–64. https://doi.org/10.1016/j.enconman.2013.07.076.
[9] Bou Nader WS, Mansour CJ, Nemer MG, Guezet OM. Exergo-technological explicit methodology for gas-turbine system optimization of series hybrid electric vehicles. Proceedings of the Institution of Mechanical Engineers, Part D: Journal of Automobile Engineering. 2018;232(10):1323–38. https://doi.org/10.1177/0954407017728849.
[10] Bou Nader W, Cheng Y, Nault E, Reine A, Wakim S, Kabalan B, et al. Technological analysis and fuel consumption saving potential of different gas turbine thermodynamic configurations for series hybrid electric vehicles. Proceedings of the Institution of Mechanical Engineers, Part D: Journal of Automobile Engineering. 2020;234(6):1544–62. https://doi.org/10.1177/0954407019890160.
[11] Reine A, Bou NW. Fuel consumption potential of different external combustion gas-turbine thermodynamic configurations for extended-range electric vehicles. Energy. 2019;175:900–13. https://doi.org/10.1016/j.energy.2019.03.076.
[12] Bou Nader W, Breque F, Mazloum Y, Dumand C, Nemer M. Dynamic Modeling and Fuel Consumption Potential of an Intercooled Regenerative Reheat Gas Turbine Auxiliary Power Unit on Series Hybrid Electric Vehicle. J Energy Res Technol 2020;142(1):1–18. https://doi.org/10.1115/1.4044366.
[13] NASA Technical Note. Michael R. Galvas. Analytical correlation of centrifugal compressor design geometry for maximum efficiency with specific speed. National aeronautics and space administration. Washington, D. C. March 1972.
[14] NASA Technical Note. Harold E. Rohlik. Analytical determination of radial inflow turbine design geometry for maximum efficiency. National aeronautics and space administration. Washington, D. C. February 1968.
[15] Tiainen J, Jaatinen-Värri A, Grönman A, Fischer T, Backman J. Loss development analysis of a micro-scale centrifugal compressor. Energy Convers Manage 2018;166:297–307. https://doi.org/10.1016/j.enconman.2018.04.014.
[16] Bayomi NN. Radial Turbine Design Process. ISESCO Journal of Science and Technology. 2015; (MAY):199-327. http://www.conceptsnrec.com/Education/Engineering-Textbooks.aspx.
[17] Gutiérrez Velásquez EI. Determination of a suitable set of loss models for centrifugal compressor performance prediction. Chin J Aeronaut 2017;30(5):1644–50. https://doi.org/10.1016/j.cja.2017.08.002.
[18] Rusch D, Casey M. The design space boundaries for high flow capacity centrifugal compressors. J Turbomach 2013;135(3):1–11. https://doi.org/10.1115/1.4007548.
[19] Shah Samip. Effect of flow coefficient and loading coefficient on the radial inflow turbine impeller geometry. Int J Res Eng Technol 2013;02(02):98–104. https://doi.org/10.15623/ijret10.15623/ijret.2013.0202002.
[20] Rodgers C, Sapiro L. "Design Considerations for High Pressure Ratio Centrifugal Compressors," ASME, 72-GT91 doi:10.1038/sj.eye.6700335.
[21] Pierre-Thomas Lauriau et al. Preliminary Design Considerations for Variable Geometry Radial Turbines with Multi-Points Specifications. https://doi.org/10.3390/ijtpp3040022.
[22] Ramesh K. Shah and Dusan P. Sekulic. FUNDAMENTALS OF HEAT EXCHANGER DESIGN. Rochester Institute of Technology, Rochester, New York.